journal of the mechanical behavior of biomedical materials 140 (2023) 105740

Contents lists available at ScienceDirect

Journal of the Mechanical Behavior of Biomedical Materials

journal homepage: www.elsevier.com/locate/jmbbm

Accuracy of osseointegrated screw-bone construct stiffness and peri-implant loading predicted by homogenized FE models relative to micro-FE models

Alexander Synek [a,*], Lukas Ortner [a], Dieter H. Pahr [a,b]

[a] Institute of Lightweight Design and Structural Biomechanics, TU Wien, Austria
[b] Division Biomechanics, Karl Landsteiner University of Health Sciences, Austria

ARTICLE INFO

Keywords:
Screw
Bone
Interface
Homogenized
Finite element
Micro-FE

ABSTRACT

Computational predictions of stiffness and peri-implant loading of screw-bone constructs are highly relevant to investigate and improve bone fracture fixations. Homogenized finite element (hFE) models have been used for this purpose in the past, but their accuracy has been questioned given the numerous simplifications, such as neglecting screw threads and modelling the trabecular bone structure as a continuum. This study aimed to investigate the accuracy of hFE models of an osseointegrated screw-bone construct when compared to micro-FE models considering the simplified screw geometry and different trabecular bone material models.

Micro-FE and hFE models were created from 15 cylindrical bone samples with a virtually inserted, osseointegrated screw (fully bonded interface). Micro-FE models were created including the screw with threads (=reference models) and without threads to quantify the error due to screw geometry simplification. In the hFE models, the screws were modelled without threads and four different trabecular bone material models were used, including orthotropic and isotropic material derived from homogenization with kinematic uniform boundary conditions (KUBC), as well as from periodicity-compatible mixed uniform boundary conditions (PMUBC). Three load cases were simulated (pullout, shear in two directions) and errors in the construct stiffness and the volume average strain energy density (SED) in the peri-implant region were evaluated relative to the micro-FE model with a threaded screw.

The pooled error caused by only omitting screw threads was low (max: 8.0%) compared to the pooled error additionally including homogenized trabecular bone material (max: 92.2%). Stiffness was predicted most accurately using PMUBC-derived orthotropic material (error: -0.7 ± 8.0%) and least accurately using KUBC-derived isotropic material (error: +23.1 ± 24.4%). Peri-implant SED averages were generally well correlated ($R^2 \geq 0.76$), but slightly over- or underestimated by the hFE models and SED distributions were qualitatively different between hFE and micro-FE models.

This study suggests that osseointegrated screw-bone construct stiffness can be predicted accurately using hFE models when compared to micro-FE models and that volume average peri-implant SEDs are well correlated. However, the hFE models are highly sensitive to the choice of trabecular bone material properties. PMUBC-derived isotropic material properties represented the best trade-off between model accuracy and complexity in this study.

1. Introduction

Internal fixation with plates and screws has become a popular treatment method for complex bone fractures (Azad et al., 2019; Li et al., 2020). However, mechanical failures are still reported (Kralinger et al., 2014; Li et al., 2019) and there is an increasing demand for optimization to reduce treatment costs (Kazmers et al., 2018). Biomechanical simulations could help to further improve fracture fixations and even enable optimized, patient-specific treatment in the future (Lewis et al., 2021). These simulations have mainly been performed using two kinds of models: micro-finite element (micro-FE) models and homogenized FE (hFE) models. Micro-FE models include the microstructural geometry of

* Corresponding author. Gumpendorfer Straße 7, Institute of Lightweight Design and Structural Biomechanics, 1060, Vienna, Austria.
E-mail address: asynek@ilsb.tuwien.ac.at (A. Synek).

https://doi.org/10.1016/j.jmbbm.2023.105740
Received 21 December 2022; Received in revised form 9 February 2023; Accepted 21 February 2023
Available online 22 February 2023

the bone and have achieved good agreement with experimental results (Steiner et al., 2018), but they are computationally demanding and rely on high resolution computed tomography (CT) scans which are hardly available in vivo. hFE models are a promising alternative as they are computationally efficient and could be created based on clinically available CT scans.

However, the accuracy of hFE models of screw-bone constructs has been questioned particularly if the screws are anchored in trabecular bone (Einafshar et al., 2021; Wirth et al., 2012). In hFE models, bone is modelled as a continuum despite its complex microstructure, and screw geometries are often simplified (e.g. as cylinders without threads) to maintain computational efficiency (Caiti et al., 2019; Ovesy et al., 2018; Synek et al., 2015; Varga et al., 2017). Given these simplifications, some studies suggested that hFE models are of limited use to simulate screw-bone construct mechanics, reporting inaccuracies of peri-implant loading, structural stiffness and failure loads of a single screw in porous bone or bone surrogate material (Einafshar et al., 2021; Wirth et al., 2012). A previous study on an entire distal radius fracture fixation showed that hFE-predicted construct stiffness correlates well with experimental data, but is overestimated by the models (Synek et al., 2015). Interestingly, volume averaged peri-implant strain of hFE models was found to be well-correlated with fatigue failure of proximal humerus fracture fixations (Varga et al., 2017), even though the peri-implant load distribution was repeatedly reported to be inaccurate in hFE models (Chevalier, 2015; Wirth et al., 2012). Thus, hFE models seem to deliver useful correlates with clinically relevant biomechanical parameters, but their accuracy is still debated and different error sources remain to be disentangled.

An arguably large error source in hFE models of screw-bone constructs is to model bone as a continuum with homogenized material properties. Bone is an inhomogeneous material with a dense cortical shell surrounding the highly porous trabecular bone. To account for this inhomogeneity, cortical and trabecular bone phases are typically separated in hFE models (Caiti et al., 2019; Synek et al., 2021) and material mapping can be used to account for spatial variation of the material properties (Kim et al., 2020; Synek et al., 2015). Various different bone material models and constants have been used in previous studies, ranging from homogeneous isotropic (Caiti et al., 2019; Knežević et al., 2017) to inhomogeneous, density and fabric dependent material (Synek et al., 2015). While the effect of different homogenized bone material models is well documented for intact bone (Helgason et al., 2016; Marangalou et al., 2012; Pahr and Zysset, 2009), only few studies investigated their influence in hFE simulations of screw-bone constructs (Synek et al., 2015; Varga et al., 2017). It remains unclear which bone material models and constants are best suited for accurate predictions of the mechanical behaviour of screw-bone constructs with hFE models, and how strong the choice of material model affects the accuracy of the predictions.

Another potential error source in hFE models of screw-bone constructs is the interface between the bone and the screws. In case primary stability should be investigated, bone damage due to screw insertion and screw-bone contact are critical modelling aspects (Steiner et al., 2015, 2017). Implementing these phenomena in hFE models is challenging and conflicting results about their accuracy have been reported (Einafshar et al., 2021; Ovesy et al., 2018). But even in the osseointegrated case, i.e. assuming a fully bonded screw-bone interface (Steiner et al., 2015; Wirth et al., 2011), hFE models might not be able to accurately capture the mechanical behaviour of screw-bone constructs. For instance, Wirth et al. (2012) used micro-FE models of trabecular bone with a virtually inserted, osseointegrated screw as a reference and found poor agreement of stiffness and peri-implant strains to hFE models in a simulated pullout load case. Chevalier (2015) reported that hFE models accurately captured the elastic structural response of an osseointegrated screw in trabecular bone when compared to micro-FE models, but still observed differences in peri-implant stress distributions. In both of these studies, the error due to simplified screw threads in hFE models has not yet been considered. Moreover, Chevalier (2015) and Wirth et al. (2012) included only trabecular bone in their studies, whereas the screw is typically anchored in both cortical and trabecular bone in a clinical scenario. Overall, the literature is inconclusive about the accuracy of hFE models of screw-bone constructs, even for the simple case of linear elastic bone material and a single, fully osseointegrated screw.

The main goal of this study was to assess the accuracy of hFE-predicted stiffness and peri-implant loading of bone with an osseointegrated screw, using micro-FE models as reference. The first subgoal was to delineate different error sources in hFE models (simplified screw geometry, homogenized bone material) and the second subgoal was to compare the accuracy achieved with different trabecular bone material models. To ensure clinical relevance, the bone samples included both cortical and trabecular bone and the accuracy was evaluated for multiple load cases.

2. Methods

2.1. Study outline

Fig. 1 presents an outline of the study. In brief, 15 cylindrical bone specimens with 18 mm diameter were extracted from micro-CT scans of human distal radii and a screw was virtually inserted. Linear elastic micro-FE models with perfectly bonded screw-bone interface ("osseointegrated") and screws including the thread geometry were created as reference models. In order evaluate the error due to simplified screw threads, an additional set of micro-FE models substituting the threaded screw with a smooth cylinder was created and compared to the micro-FE model with threads. Smooth hFE models were created with separated cortical and trabecular bone phases and the simplified screw geometry without threads. Four different trabecular bone material models were used, derived either from micro-FE-based homogenization with kinematic uniform boundary conditions (KUBC) or periodicity-compatible mixed uniform boundary conditions (PMUBC) and assuming either isotropy (KUBC-iso, PMUBC-iso) or orthotropy (KUBC-ortho, PMUBC-ortho) (Pahr and Zysset, 2009; Panyasantisuk et al., 2015). Three load cases were simulated by applying a force along the screw axis (pullout) and in two directions perpendicular to the screw axis (shear). Structural stiffness and volume-average strain energy density (SED) in the peri-implant region were evaluated for all load cases to assess the accuracy of the hFE models with respect to the micro-FE models with screw threads.

2.2. Image processing

15 micro-CT scans of human distal radii (l/r: 8/7; f/m: 5/10) resampled to 32.8 μm resolution were obtained from two previous studies (Hosseini et al., 2017; Stipsitz et al., 2021). The original micro-CT scans were taken by Hosseini et al. (2017) from 20 mm high distal radius sections of body donors (age: 77.5 ± 9 years) using a μCT 100 scanner (SCANCO Medical AG, Brüttisellen, Switzerland) with a resolution of 16.4 μm. Images resampled to 32.8 μm resolution, bone segmentations and masks covering the trabecular and cortical bone phases were directly taken from Stipsitz et al. (2021). All images were rotated to ensure uniform alignment of the volar surface and a cylindrical region with 18 mm diameter was cropped from the center of the bone (Fig. 2). The diameter of this region was chosen as large as possible, given the constraints of scan height and specimen width, to reduce the effect of boundary conditions on the peri-implant load distribution. A micro-CT scan of a locking screw of a distal radius fracture fixation system (A-5750; Medartis, Basel, Switzerland; outer diameter: 2.5 mm) was obtained using a micro-CT scanner (Skyscan 1173; Bruker, Bilerica, USA) at 21.9 μm resolution. The image was rescaled to 32.8 μm resolution, segmented, aligned along the screw axis and cut to 15 mm length. The screw was then inserted into the center of each micro-CT image of segmented bone with an insertion depth of 10 mm (Fig. 2). The insertion

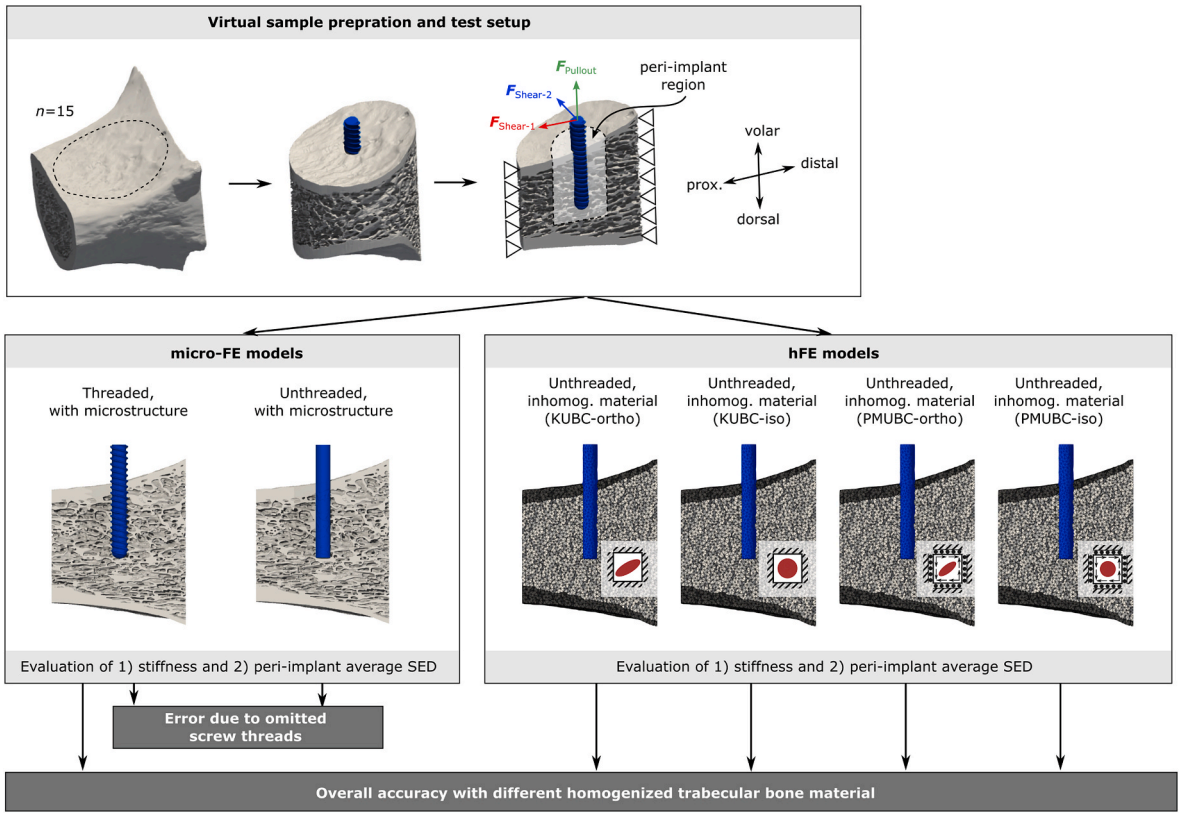

Fig. 1. Outline of the study. 15 cylindrical bone samples from distal radii with virtually inserted screws were modelled using micro-FE and hFE methods. hFE models were created with four different trabecular bone material models model (KUBC-ortho, KUBC-iso, PMUBC-ortho, PMUBC-iso) to evaluate the overall accuracy of the hFE models and to influence of the chosen material (shown in sagittal cross sections of the cylindrical sample in the second row). An additional set of micro-FE models without screw threads was created to evaluate the effect of simplified screw geometry. All models were compared in three load cases (axial pullout; shear in two directions) based on the structural stiffness and volume-average peri-implant strain energy density (SED) in the peri-implant region.

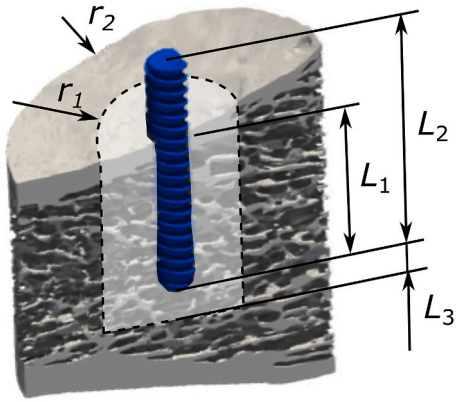

Fig. 2. Virtual sample preparation and sample dimensions. The cylindrical bone sample had a radius of $r_2 = 9$ mm. The inserted screw had a length of $L_2 = 15$ mm and an insertion depth of $L_1 = 10$ mm. The peri-implant region was defined as a cylindrical region around the screw with a diameter of $r_1 = 4$ mm and an offset from the tip of $L_3 = 2$ mm.

depth was chosen to simulate unicortical fixation, which is typical for distal screws in volar locking plate fixation (Baumbach et al., 2015). For the hFE models, a cylinder was created to represent the unthreaded screw and inserted into the 3D images of the trabecular and cortical bone masks. The diameter was calculated as 1.99 mm following the assumption of consistent average cross-sectional area of the screw and the cylinder. An additional set of images was created for the micro-FE model without screw threads by inserting the cylinder into the segmented bone images. All image processing steps were conducted in Medtool 4.5 (Dr. Pahr Ingenieurs e.U., Pfaffstätten, Austria).

2.3. Morphometry

Since the error in homogenized material properties may depend on bone morphometry (Pahr and Zysset, 2008), standard morphometric parameters were evaluated from the cylindrical bone samples prior to screw insertion (Supplemental Table S1). Mean cortical thickness was only evaluated for the volar cortex and ranged from 0.5 to 1.07 mm. Trabecular bone volume fractions ranged from 9 to 26% and the degree of anisotropy was high in all samples, ranging from 1.7 to 2.19. The trabecular structure was strongly aligned with the proximo-distal direction (see Figs. 1 and 2).

2.4. Micro-FE modelling

Micro-FE models were created based on the segmented bone images with either the threaded or unthreaded screw. The mesh was created by directly converting each voxel to an eight-noded hexahedral element, resulting in an element edge length of 32.8 μm. The bone tissue was modelled with an elastic modulus of 12 GPa (Gross et al., 2013) and the titanium alloy screw was modelled with an elastic modulus of 115 GPa (Synek et al., 2021), both with a Poisson's ratio of 0.3. All nodes at the cylindrical boundary of the bone were fixed and load was applied to the most volar surface of the screw (Fig. 1). Three load cases were simulated: In the pullout load case, a force of 100 N was applied in volar direction, and for the two shear load cases, a total force of 100 N was applied in either proximal or radial/ulnar direction. All models were created using Medtool, had 108.4 ± 28.4 million degrees of freedom (DoF), and were

solved using ParOSol (Flaig and Arbenz, 2011; Stipsitz et al., 2020).

2.5. hFE modelling

Smooth hFE models were created by meshing the 3D images containing the trabecular and cortical bone masks as well as a cylinder representing the unthreaded screw. Meshes with second order tetrahedral elements and an approximate element size of 0.4 mm were created using Medtool and the computational geometry algorithms library (CGAL) (Alliez et al., 2014). The element size was chosen following a mesh convergence study (see Appendix A).

Bone material properties were assigned to each element using a previously presented material mapping algorithm (Pahr and Zysset, 2009). In brief, the algorithm evaluates the relative bone density ρ and the fabric tensor within multiple sampling spheres in a regular grid and assigns their interpolated values to each element. In this study, the sampling sphere size was set to 5 mm, the grid spacing was set to 2.5 mm and the fabric tensor was established using the mean intercept length method. Density and fabric tensors are then used to compute material properties for each element as described below.

The cortical bone material was modelled using an isotropic density dependent power law:

$$E = E_0 \rho^k$$

where E is the elastic modulus and E_0 and k are material constants. E_0 was set to 12 GPa to ensure consistency with the micro FE models, k was set to 2 following Rice et al. (1988), and the Poission's ratio was set to 0.3. For the trabecular bone in the KUBC-iso and PMUBC-iso models, an isotropic power law in analogy to the cortex was used. Respective material constants were obtained based on a previous study (Panyasantisuk et al., 2015), but rescaled to a bone tissue elastic modulus of 12 GPa to ensure consistency with the micro-FE models (Table 1). For the KUBC-ortho and PMUBC-ortho models, a Zysset-Curnier type orthotropic trabecular bone model was used (Panyasantisuk et al., 2015; Zysset and Curnier, 1995):

$$E_i = E_0 \rho^k m_i^{2l}$$

$$G_{ij} = G_0 \rho^k m_i^l m_j^l$$

$$\nu_{ij} = \nu_0 \frac{m_j^l}{m_i^l}$$

Where E_0, G_0, ν_0, k and l are material constants, and m_i are the eigenvalues of the fabric tensor. The material constants were taken from the same study as for the isotropic trabecular bone material (Panyasantisuk et al., 2015) and also rescaled to match the bone tissue elastic modulus of the micro-FE models. The titanium alloy screw was modelled with an elastic modulus of 115 GPa and a Poisson's ratio of 0.3 in analogy to the micro-FE models.

The boundary conditions were applied to the hFE models in a similar way to the micro-FE models, i.e. all nodes at the cylindrical boundary were constrained and a force of 100 N was applied to the screw to simulate pullout or shear loading (Fig. 1). To facilitate load application and data evaluation, a reference point was coupled to all nodes of the volar surface of the screw.

In order to verify the hFE model solution and to ensure that errors from boundary conditions and meshing do not influence the comparison between hFE and micro-FE models, hFE and micro-FE models with homogeneous cortical and trabecular bone regions and an unthreaded screw were created and compared based on all output variables used in this study (see Appendix B for details). Overall, the error was less than 5% for all load cases and variables.

All hFE models were created using Medtool, had 1.1 ± 0.1 million DoF, and were solved using Abaqus (2021HF3; Dassault Systemes, Velizy-Villacoublay, France).

Table 1
Material constants used for the trabecular bone models of the hFE models. The constants were determined based on (Panyasantisuk et al., 2015) *but rescaled for the tissue elastic modulus of the micro-FE models used in this study.*

hFE model type	E_0 (MPa)	G_0 (MPa)	ν_0 (−)	k (−)	l (−)
KUBC-ortho	9381.77	3426.17	0.2320	1.55	0.84
KUBC-iso	8556.24	–	0.2426	1.55	–
PMUBC-ortho	13757.76	4136.17	0.2228	2.01	1.20
PMUBC-iso	10904.96	–	0.2526	2.00	–

2.6. Output variables

The main output variables of the simulations were: 1) The stiffness of the entire screw-bone structure and 2) the volume-average SED in the peri-implant region. Stiffness was chosen as it, along with implant plate bending, contributes to accurate predictions of fracture gap motion in models of entire fracture fixations. In addition, screw-bone construct stiffness may influence the force transmission to the implant plate. Volume-average SED in the peri-implant region was chosen for two reasons. First, volume-average peri-implant loading may be a good predictor of fatigue failure of screw-bone constructs as indicated in a previous study (Varga et al., 2017). Second, it allows to evaluate the agreement of the elastic energy stored in the peri-implant bone between the micro-FE and hFE models.

Stiffness in the pullout and shear load cases was defined as the applied force F divided by the displacement u in the respective direction i:

$$K_i = \frac{F_i}{u_i}$$

In the micro-FE models, u_i was the averaged displacement in direction i of the most volar node set of the screw. In the hFE models, u_i was the displacement of the reference node in direction i.

The peri-implant volume-average SED $\langle U \rangle$ was evaluated in a cylindrical region around the screw with a radius of 4 mm and extending 2 mm beyond the screw tip (Fig. 2). In the micro-FE models, all n elements within the peri-implant region were selected and $\langle U \rangle$ was computed as:

$$\langle U \rangle = \frac{1}{V_{\text{Total}}} \sum_{i=1}^{n} U_i \, V_i$$

where U_i is the SED at the element centroid, V_i is the respective element volume, and V_{Total} is the total volume of the peri-implant region including both bone and void volume. In the hFE models, U_i and V_i were evaluated at the element integration points. Note that the peri-implant region size affects the absolute values of $\langle U \rangle$. Additional evaluations with differently sized peri-implant regions were conducted to ensure that the main findings of this study are not limited to a single peri-implant region size (Appendix C).

2.7. Comparison of hFE and micro-FE models

The micro-FE and hFE models were compared qualitatively based on their deformation and the spatial distribution of SEDs in the three load cases.

In order to address the first subgoal, i.e. to delineate different error sources, the pooled error (all load cases) of the stiffness and volume-average peri-implant SED was evaluated. The pooled errors were split into the error due to omitting screw threads and the overall error including the hFE models with the four different trabecular bone material models. Errors of each variable were defined as the difference of hFE and micro-FE, relative to the micro-FE models with screw threads.

To address the second subgoal, i.e. to investigate the overall accuracy of the hFE models with different trabecular bone material models, the

relative error and Lin's Concordance Correlation Coefficient (*CCC*) (Lin, 1989) was evaluated. The hFE models were considered accurate if the mean error of the pooled data was close to zero, and the *CCC* was above 0.95, indicating a "substantial" agreement (Akoglu, 2018). In addition to the pooled data, relative errors and *CCC* were assessed for each individual load case. Furthermore, the correlation of the results was evaluated in terms of the coefficient of determination (R^2).

All descriptive statics are presented as mean ± standard deviation (SD) if not noted differently and all correlation analyses were performed using SciPy (Virtanen et al., 2020). The statistical significance of differences between errors was evaluated with Friedman tests and Dunn-Bonferroni post-hoc tests using SPSS (v27; IBM Corporation, New York, USA) with a level of significance of 5%.

3. Results

3.1. Qualitative comparison of deformation and SED distributions

The qualitative comparison of deformation and SED distributions of the three load cases is shown for one representative specimen in Fig. 3. Differences in SED distributions between threaded and unthreaded micro-FE models were small and restricted to regions in close proximity to the screw. Large differences were visible between the micro-FE and all hFE models, but only minor differences were observed between hFE models with different trabecular bone material models.

Qualitatively, a better agreement between micro-FE and hFE models was achieved in the shear load cases when compared to the pullout load case, as well as a better agreement in the cortical when compared to the trabecular bone. In the pullout load case, SEDs were particularly high below the tip of the screw in the hFE models, whereas the SEDs were more evenly distributed along the screw shaft in the micro-FE models.

3.2. Delineation of error sources and pooled errors

The analysis of the pooled errors of all load cases revealed that the error caused by simplified screw geometry alone was relatively low (overall range: -7.3 to 8.0%) compared to the error including both simplified screw geometry and homogenized bone material (overall range: -54.4 to 92.2%) (Fig. 4, Table 2). The mean error caused by omitting screw threads was within ±5% for both predicted stiffness and peri-implant average SED.

Significant differences of the pooled errors were observed for the hFE models with different trabecular bone material (Fig. 4, Table 2). In particular, the errors were significantly different between KUBC- and PMUBC-derived material properties both for the isotropic and orthotropic models. In terms of stiffness, using orthotropic PMUBC-derived material properties led to the lowest errors (−0.7 ± 8.0%) and using KUBC-derived isotropic bone material led to largest errors (+23.1 ± 24.4%). hFE models with PMUBC-derived bone material had a mean error of the predicted stiffness within ±5%, whereas KUBC-derived bone material led to an overestimation of the stiffness. Volume average SEDs in the peri-implant region were slightly overestimated using PMUBC-derived and underestimated using KUBC-derived material properties. A minor, statistically insignificant reduction of the pooled errors was achieved using orthotropic rather than isotropic bone material.

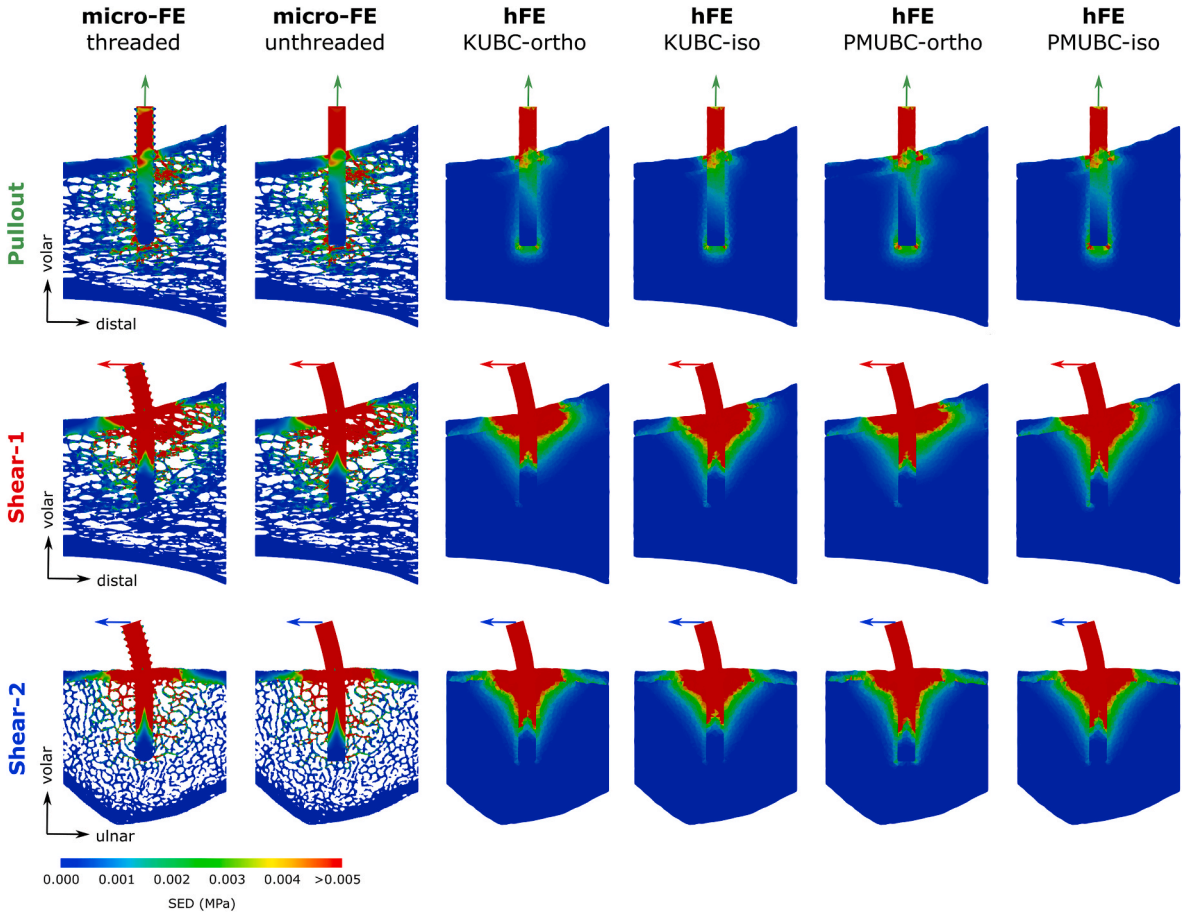

Fig. 3. Qualitative comparison of deformation and SED distributions of different micro- and hFE models for one representative sample in the pullout and shear load cases. Pullout and shear-1 load cases are shown as sagittal cross sections, while the shear-2 load case is shown in a transverse cross section. For visualization, the deformations were scaled by a factor of ten.

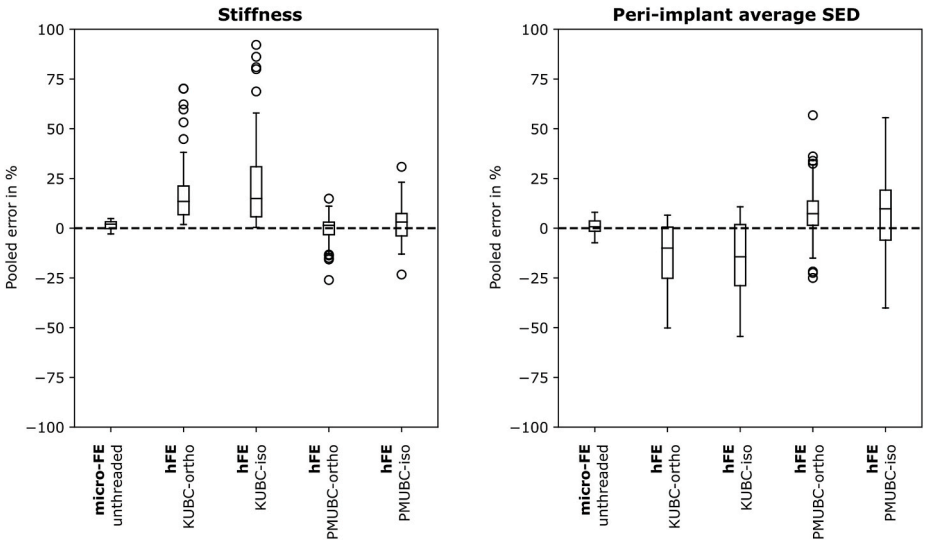

Fig. 4. Pooled errors of various models relative to the micro-FE model with screw threads in terms of stiffness and volume average SED in the peri-implant region.

Table 2
Mean errors and standard deviations of the homogenized models with respect to the micro-FE models of all load cases and the pooled data including all load cases. SD: Standard deviation.

Variable	Load case	KUBC-ortho		KUBC-iso		PMUBC-ortho		PMUBC-iso	
		Mean	SD	Mean	SD	Mean	SD	Mean	SD
Stiffness error (%)	Pullout	36.37	21.56	47.65	26.77	−7.53	9.42	1.94	14.14
	Shear-1	6.61	4.54	4.86	4.26	0.78	3.22	−2.70	3.11
	Shear-2	14.04	8.15	16.73	8.86	4.56	4.03	8.90	5.39
	Pooled	19.01	18.54	23.08	24.42	−0.73	8.00	2.71	10.11
Peri-implant average SED error (%)	Pullout	−16.00	12.40	−22.43	13.74	24.91	13.70	15.57	17.57
	Shear-1	−5.07	11.89	−0.21	11.86	2.77	8.67	14.53	9.01
	Shear-2	−17.50	17.06	−21.17	17.51	−1.43	11.79	−11.26	13.73
	Pooled	−12.86	15.04	−14.60	17.78	8.75	16.35	6.28	18.62

3.3. Errors of hFE model predictions for each load case

For all material models and output parameters, significant differences between the errors of different load cases were found. The errors between micro-FE and hFE models were overall lower in the shear load cases when compared to the pullout load case (Fig. 5, Table 2). This was particularly pronounced in the hFE models with KUBC-derived material properties, which strongly overestimated the pullout stiffness. The stiffness error of the hFE models with PMUBC-derived material was less variable between the different load cases. Differences in the error between the two shear load cases were more pronounced in the models with isotropic bone material when compared to the models with orthotropic bone material.

3.4. Correlations of hFE with micro-FE model predictions

Correlations between micro- and hFE model predictions were generally good to excellent for all load cases and all output variables (R^2: 0.76 to 0.99) (Fig. 6, Table 3). hFE models with PMUBC-derived trabecular bone material generally led to a better 1:1 agreement with the micro-FE models (*CCC*: 0.65 to 0.99) when compared to KUBC-derived material (*CCC*: 0.3 to 0.95). Using PMUBC-derived orthotropic material led to the best results, with *CCC* higher than 0.95 for the pooled stiffness and volume average peri-implant SED. Using orthotropic trabecular material models generally led to a slightly higher coefficient of determination and better 1:1 agreement compared to the isotropic material models.

4. Discussion

The primary goal of this study was to assess the accuracy of hFE predicted stiffness and peri-implant loading of bone with an osseointegrated screw, using micro-FE models as a reference. The results showed that not only well-correlated but also accurate predictions of pullout and shear stiffness are possible with hFE models, provided that appropriate trabecular bone material properties are chosen. PMUBC-derived orthotropic trabecular bone material properties led to the best results in this study (mean pooled error: -0.7%, *CCC*: 0.98). However, qualitative differences in the peri-implant SED distributions were evident in all hFE models, and although the peri-implant SED averages were well correlated, small systematic errors were still observed.

The results of this study can be compared with two previous studies (Chevalier, 2015; Wirth et al., 2012) that also assessed the accuracy of hFE models of osseointegrated screw-bone constructs relative to micro-FE models. In line with Chevalier (2015), this study suggests that accurate predictions of stiffness are possible with hFE models even for different load cases. While Chevalier only tested trabecular bone specimens without a cortical shell, the results found in this study showed that accurate stiffness predictions are also possible with hFE models for the clinically more relevant scenario of a thin cortex covering the trabecular bone. In contrast to Chevalier (2015) and the present study, Wirth et al. (2012) reported a considerable mismatch of pullout stiffness between hFE and micro-FE models. This mismatch might be the result of using a single elastic modulus for the entire peri-implant region rather than material mapping, or of determining the elastic modulus from uniaxial compression tests rather than material homogenization in their study

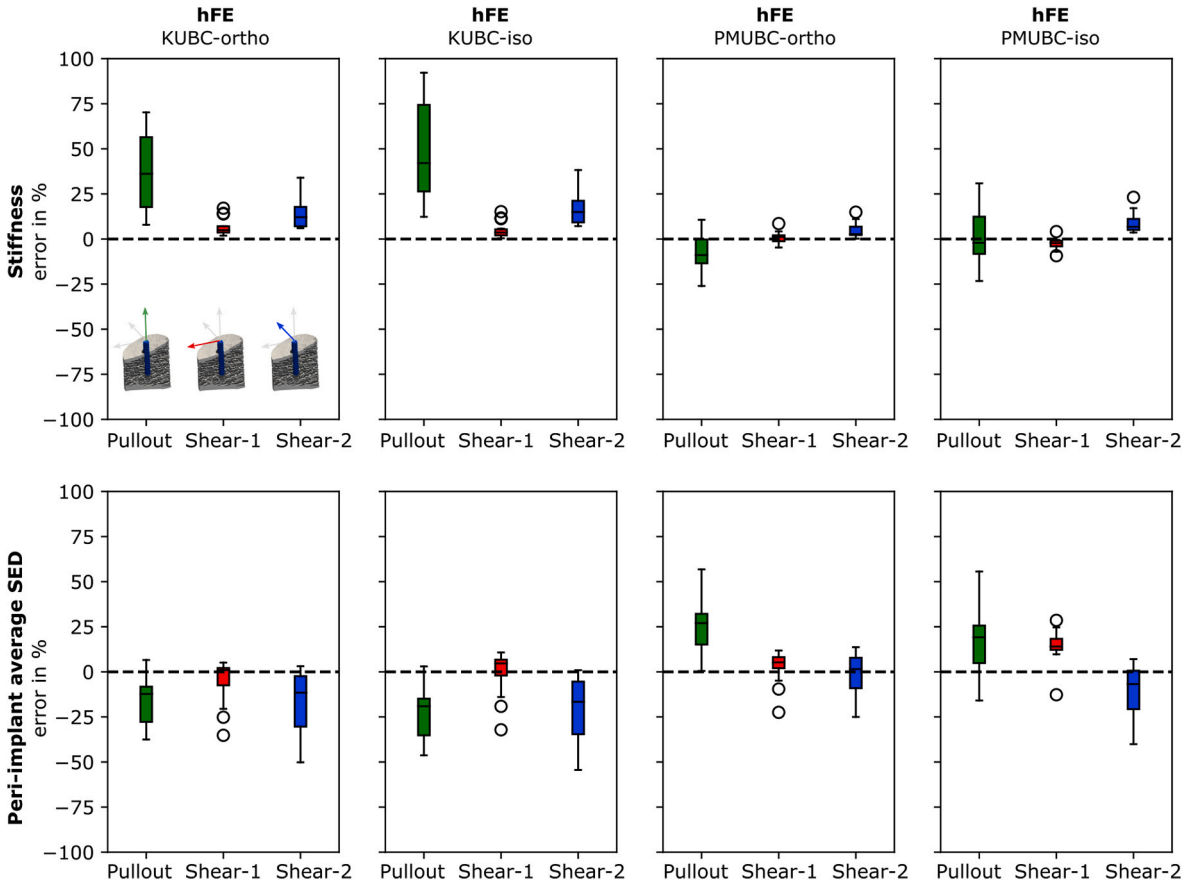

Fig. 5. Relative error of the hFE models with respect to the micro-FE models for stiffness and volume average peri-implant SED in the pullout and shear load case. For the pooled errors, the reader is referred to Fig. 4.

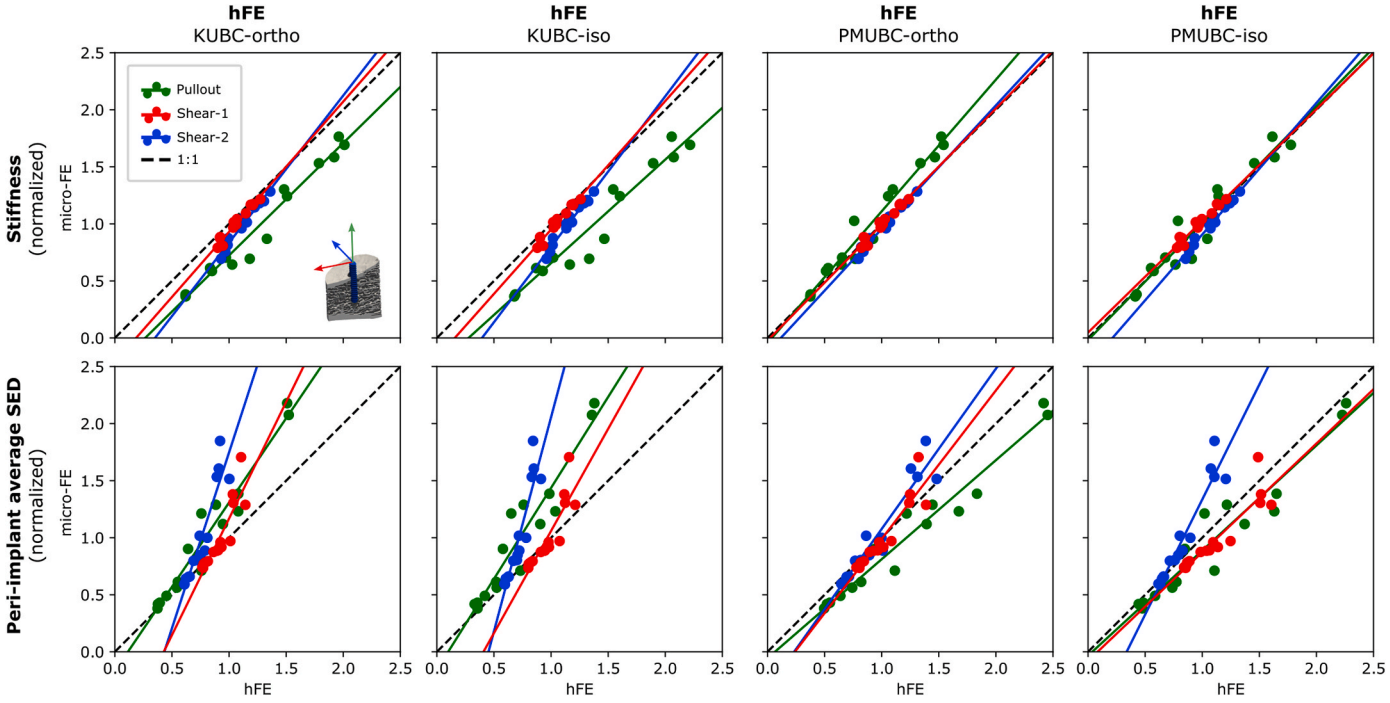

Fig. 6. Correlations between micro-FE (y-axis) and hFE (x-axis) model predictions of structural stiffness and peri-implant volume average SEDs with different trabecular material modelling approaches. Each variable was normalized by the mean of the micro-FE model prediction to facilitate the visual comparison.

Table 3
Concordance correlation coefficients (*CCC*) and coefficient of determination (R^2) of all load cases and the pooled data including all load cases.

Variable	Load case	KUBC-ortho		KUBC-iso		PMUBC-ortho		PMUBC-iso	
		CCC	R^2	*CCC*	R^2	*CCC*	R^2	*CCC*	R^2
Stiffness	Pullout	0.83	0.95	0.73	0.92	0.95	0.97	0.96	0.93
	Shear-1	0.87	0.96	0.91	0.96	0.98	0.96	0.96	0.96
	Shear-2	0.72	0.97	0.64	0.97	0.96	0.98	0.87	0.98
	Pooled	0.95	0.98	0.92	0.97	0.98	0.99	0.99	0.98
Peri-implant average SED	Pullout	0.82	0.95	0.71	0.91	0.91	0.96	0.94	0.92
	Shear-1	0.60	0.79	0.69	0.78	0.87	0.85	0.81	0.83
	Shear-2	0.39	0.87	0.30	0.86	0.88	0.91	0.65	0.92
	Pooled	0.80	0.82	0.77	0.76	0.96	0.95	0.89	0.84

(Wirth et al., 2012). In terms of peri-implant loading, the results of the present as well as both previous studies showed inaccuracies of the spatial distribution of peri-implant loading predicted by the hFE models (i.e. distribution of stresses, strains or SEDs). Thus, micro-FE models remain the best option to investigate load transmission patterns and detailed load distributions around implants. However, the present study showed that volume averaged peri-implant SEDs of the hFE models were well correlated to micro-FE predictions. This result is reassuring for the use of volume average peri-implant loading as a predictor of fatigue failure, which has been increasingly used in the recent past (Mischler et al., 2020; Schader et al., 2022; Synek et al., 2021).

The comparison of different trabecular bone material models revealed a large impact on the hFE model accuracy. The results ranged from highly accurate predictions of structural stiffness using PMUBC-derived orthotropic material (pooled error mean ± SD: -0.7 ± 8.0%; *CCC*: 0.98), to errors up to 92% (pooled error mean ± SD: +23.1 ± 24.4%; *CCC*: 0.92) using KUBC-derived isotropic material properties. The fact that PMUBC-derived material properties generally led to higher accuracy than KUBC-derived material properties is surprising at first glance, as the stiff cortex and screw confining the trabecular bone arguably better resemble kinematic boundary conditions. However, using PMUBC for homogenization was reported to generally better approximate the effective elastic properties of trabecular bone compared to KUBC (Daszkiewicz et al., 2017; Pahr and Zysset, 2008). In addition, the shear deformation experienced by a volume element close to the screw during pullout might be better represented using PMUBCs rather than KUBCs, which would also explain the higher errors of the KUBC-derived models in this load case. Note that this is also reflected in the shear moduli, which were considerably lower in the PMUBC-derived models in the relevant range of trabecular bone density (e.g. shear moduli of the isotropic models at $\rho = 0.24$: $G_{\mathrm{KUBC}} = 376.9$ MPa vs. $G_{\mathrm{PMUBC}} = 250.7$ MPa). In terms of inclusion of the trabecular anisotropy, orthotropic material led to slightly better results compared to isotropic material. These differences were particularly visible in the comparison of shear load cases between PMUBC-derived orthotropic and isotropic models, where the isotropic model failed to capture the lower stiffness in the radio-ulnar direction (shear-2 load case). Still, the pooled mean errors were only slightly different between orthotropic and isotropic models. This is in agreement with a previous study on hFE models of an entire distal radius fracture fixation, which found only little improvement of whole construct stiffness and individual screw load predictions using orthotropic bone material (Synek et al., 2015). Thus, this study further supports the use of isotropic bone materials models for hFE models in clinical applications, which usually rely on clinical CT scans that do not allow to infer information about trabecular anisotropy.

The delineation of different error sources showed that the homogenized trabecular bone material model is a larger error source compared to neglecting screw threads. Thus, neglecting screw threads seems to be viable option for the prediction of stiffness and volume-average peri-implant loading of screw-bone constructs in case the screw is considered as osseointegrated. This is in line with a previous study on pedicle screws in vertebrae (Sensale et al., 2021), which found good agreement of predicted displacements of hFE models with fully bonded screws either with or without screw threads. Note that this result does not directly justify the use of an unthreaded screw with a fully bonded screw-bone interface to investigate primary stability, as it is done in many recent models of bone fracture fixation (Caiti et al., 2019; Synek et al., 2021). In fact, a previous study showed that there is a considerable difference in the strain field between a fully bonded screw without threads and a threaded screw with contact interaction (Inzana et al., 2016). Even though the screw threads may be omitted when simulating an osseointegrated screw, homogenized trabecular material properties must be chosen with caution to achieve accurate results. In this study, PMUBC-derived orthotropic material led to the most accurate results, but similar accuracy was achieved using PMUBC-derived isotropic material. Given the high effort of including orthotropy in hFE models, PMUBC-derived isotropic material properties might represent the best trade-off between modelling effort and accuracy. Note that this material model closely resembles a simple isotropic power law using the bone tissue elastic modulus as E_0 and an exponent of $k = 2$, which is in line with the findings of Rice et al. (1988). Thus, if the bone tissue elastic modulus is known, using a power law with an exponent of $k = 2$ seems to deliver a good approximation for the homogenized trabecular bone material properties in hFE models of screw-bone constructs.

Several limitations of this study must be mentioned. First, only osseointegrated screws were considered. Although this constitutes an important first step, the results must be interpreted separately from studies on primary stability. Future study shall extend the methodology presented in this study to enable a well-controlled hFE model validation of various mechanical aspects involved in primary stability, such as screw insertion damage and screw-bone contact (Steiner et al., 2015, 2017). Second, only four different trabecular bone material models were compared in this study. Many other material models were used in previous studies (Chevalier, 2015; Varga et al., 2017; Yan et al., 2020) and could be included in the comparison. However, using material models and constants from FE-based homogenization appeared as the most systematic and unbiased approach for this study, as they were determined using micro-FE models with consistent bone tissue elasticity following a previous study (Panyasantisuk et al., 2015) without further parameter tuning. Third, only one type of screw, unicortical fixation with a constant screw insertion depth, three load cases and one anatomical site were investigated in this study. Although this allowed a systematic comparison, the findings of this study remain to be generalized for various anatomical sites with different bone microstructure, different screw geometries, insertion depths, and load cases. Finally, it must be mentioned that micro-FE models were taken as a reference in this study, which have not been experimentally validated. Experimental validation of micro-FE models of osseointegrated screw-bone constructs were considered beyond the scope of this study, as they would require rarely available bone samples with fully ingrown screws. However, micro-FE models previously delivered predictions in very good agreement with experiments on bones without implants (Hambli, 2013;

Stipsitz et al., 2021, van Rietbergen and Ito, 2015) as well as primary stability of bone implants (Ovesy et al., 2019; Steiner et al., 2017, 2018).

In conclusion, this study suggests that construct stiffness of bone with an osseointegrated screw can be predicted accurately using hFE models when compared to micro-FE models, despite homogenized bone material properties and simplified screw thread geometry. Although peri-implant SEDs showed differences in their spatial distribution, their volume-averages were well correlated with respect to micro-FE models. However, the hFE models were highly sensitive to the choice of trabecular bone material properties. PMUBC-derived orthotropic material properties delivered the highest accuracy in this study, but PMUBC-derived isotropic material might serve as the best trade-off between accuracy and modelling effort. The latter material model closely resembles an isotropic power law using the bone tissue elastic modulus as E_0 and an exponent of $k = 2$, which might be a good first approximation in future studies.

CRediT authorship contribution statement

Alexander Synek: Writing – original draft, Visualization, Methodology, Investigation, Formal analysis, Conceptualization. **Lukas Ortner:** Writing – review & editing, Methodology, Formal analysis. **Dieter H. Pahr:** Writing – review & editing, Supervision, Software, Resources, Conceptualization.

Declaration of competing interest

The authors declare the following financial interests/personal relationships which may be considered as potential competing interests: Dieter H. Pahr is CEO of Dr. Pahr Ingenieurs e.U., which develops and distributes Medtool. All other authors declare no competing interests.

Data availability

Data will be made available on request.

Acknowledgements

We thank Juan-Diego Silva for sharing the micro-CT scan of the screw used in this study. The authors acknowledge TU Wien Bibliothek for financial support through its Open Access Funding Programme.

Appendix D. Supplementary data

Supplementary data to this article can be found online at https://doi.org/10.1016/j.jmbbm.2023.105740.

Appendix A

To ensure that the predicted stiffness and peri-implant average SEDs of the hFE models was not influenced by the selected meshing parameters, a convergence study was conducted. For this purpose, three hFE models with different meshing parameters were created for one sample with isotropic homogeneous material properties (elastic moduli of 500 MPa and 12 GPa for the trabecular and cortical bone, respectively; both with a Poisson's ratio of 0.3). The resulting meshes had 0.16 ("Mesh 1"), 1.14 ("Mesh 2") and 2.64 ("Mesh 3") million degrees of freedom (DoF). Simulations of screw pullout and two different shear load cases were performed as described in the main text, and the stiffness as well as volume-average SED in the peri-implant region were evaluated. The error of the predictions was assessed relative to the model with the finest mesh ("Mesh 3"). As shown in Figure A.1, the selected meshing parameters ("Mesh 2") resulted in errors below 2% for all load cases and output parameters.

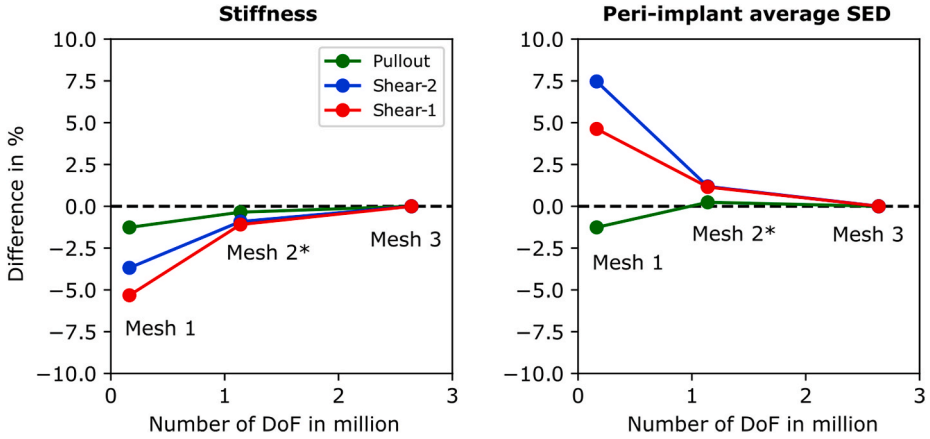

Fig. A.1. Convergence of stiffness and peri-implant average SED of hFE models of one sample with different meshes in three load cases. The meshing parameters of "Mesh 2" (marked with *) were used for all hFE models in this study.

Appendix B

To evaluate the errors introduced from the meshing or boundary conditions of the hFE models, micro-FE and hFE models were created from all 15 bone samples with homogeneous isotropic cortical and trabecular bone and a screw without thread geometry. This means that the micro-FE model was created by direct conversion of the cortical and trabecular bone masks to an FE mesh (i.e., a continuous mesh without pores or microstructure), and no material mapping was used in the hFE models. Cortical bone was assigned an elastic modulus of 12 GPa, and trabecular bone an elastic modulus of 500 MPa. Both were assigned a Poisson's ratio of 0.3. Deformation plots and SED distributions of a representative sample are shown in Figure B.1. The SED distributions were qualitatively similar and the pooled error of all 15 samples and all load cases was below 5% for both stiffness (mean ± SD: 0.1 ± 0.5%; min/max: -1.1%/+1.4%) and volume average SED in the peri-implant region (mean ± SD: 2.5 ± 1.9%; min/max: -1.1%/+4.6%).

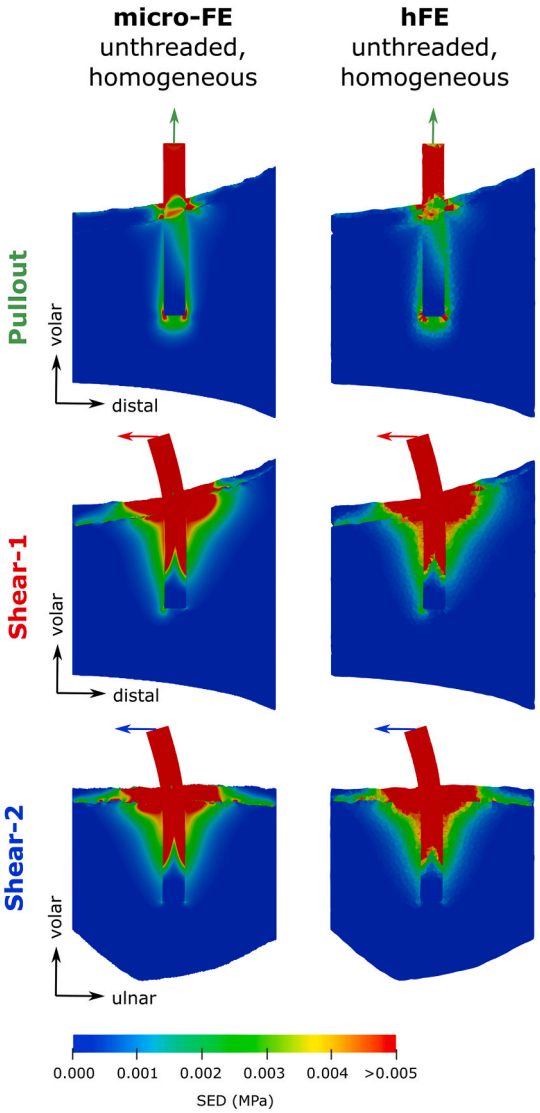

Fig. B.1. Deformation (scale factor: 10) and SED distributions of a representative specimen predicted by micro-FE and hFE methods, both with homogeneous isotropic cortical and trabecular bone material properties.

Appendix C

To ensure that the main findings of this study regarding the volume-average SEDs are not affected by the peri-implant region size, two additional peri-implant region sizes were evaluated. The original region described the main text of this manuscript had a radius of 4 mm and extended 2 mm beyond the screw tip. A smaller region was created with radius 3 mm, extending 1 mm beyond the screw tip. Additionally, a larger region with radius 5 mm and extending 3 mm beyond the screw tip was evaluated. Correlation plots were created for both the smaller and larger region and compared to the reference region in Figure C.1. The assessed parameters differed slightly (e.g. coefficients of determination), but the main trends were consistent irrespective of the peri-implant region size. The coefficient of determination (R^2) for the pooled data was larger than 0.76 for all models and region sizes (range: 0.76–0.95) and PMUBC-ortho material led to the highest correlation ($R^2 = 0.95$).

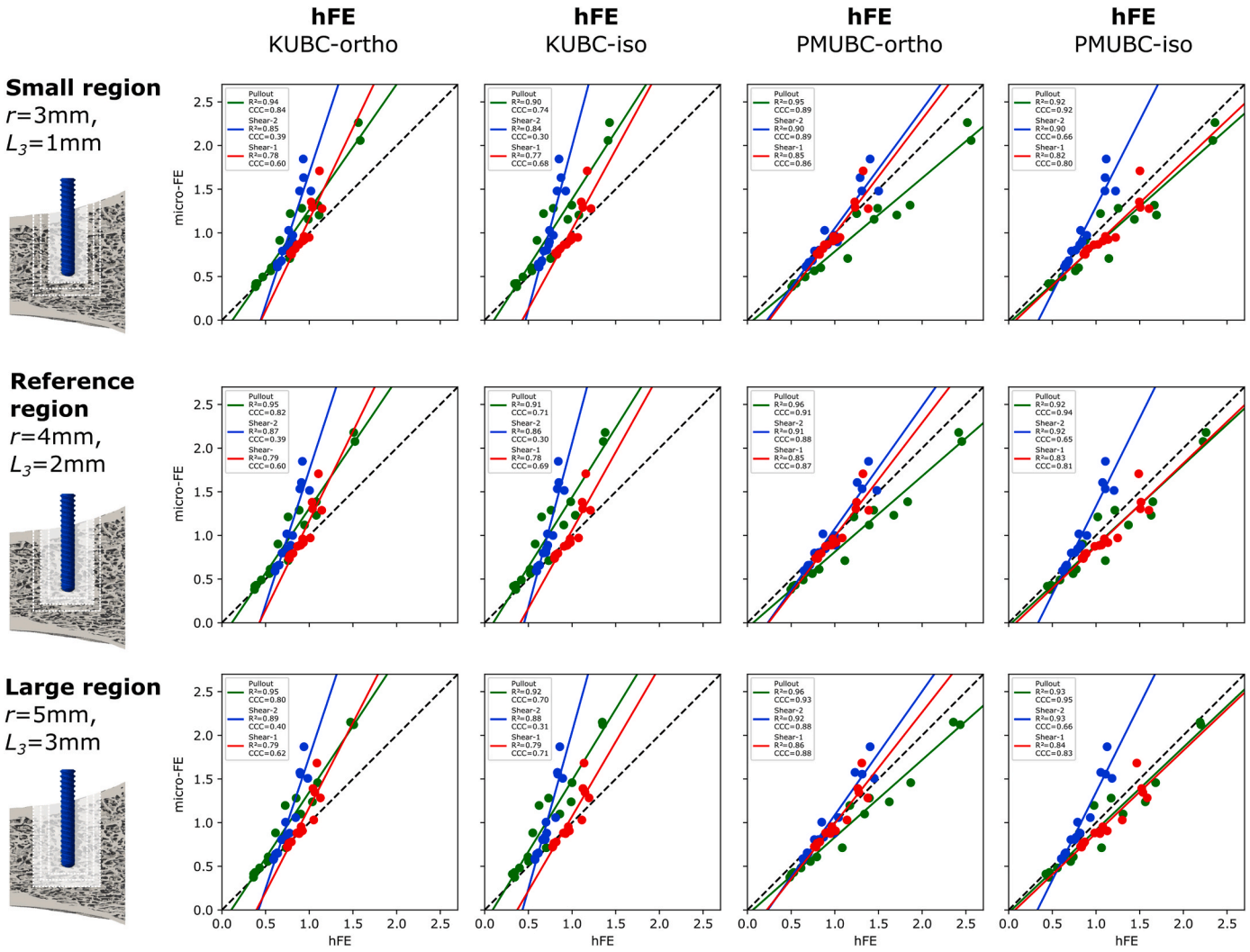

Fig. C.1. Correlations of volume average peri-implant SEDs for differently sized peri-implant regions.

The error resulting from simplified screw threads also remained fairly constant for all three peri-implant region sizes (Figure C.2), although the error increased slightly with decreasing region size (mean error, small region: 1.44%; reference region: 1.07%; large region: 0.79%).

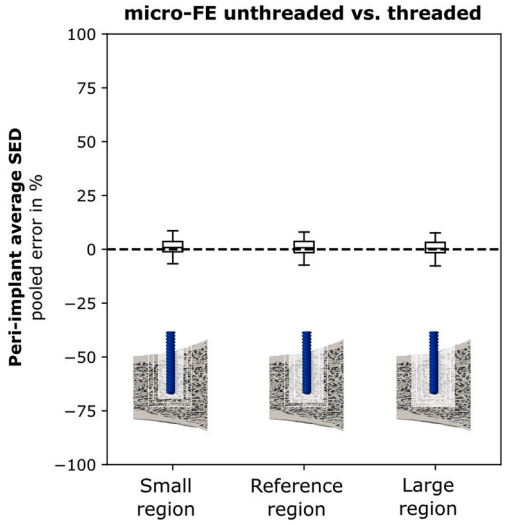

Fig. C.2. Pooled errors resulting from simplified screw threads in the micro-FE models with three different peri-implant region sizes.

References

Akoglu, H., 2018. User's guide to correlation coefficients. Turkish J. Emerg. Med. 18, 91–93. https://doi.org/10.1016/j.tjem.2018.08.001.

Alliez, P., Rineau, L., Tayeb, S., Tournois, J., Yvinec, M., 2014. 3D mesh generation. In: CGAL User and Reference Manual. CGAL Editorial Board.

Azad, A., Kang, H.P., Alluri, R.K., Vakhshori, V., Kay, H.F., Ghiassi, A., 2019. Epidemiological and treatment trends of distal radius fractures across multiple age groups. J. Wrist Surg. 305–311. https://doi.org/10.1055/S-0039-1685205, 08.

Baumbach, S.F., Synek, A., Traxler, H., Mutschler, D., Pahr, D., Chevalier, Y., 2015. The influence of distal screw length on the primary stability of volar plate osteosynthesis—a biomechanical study. J. Orthop. Surg. 10, 139. https://doi.org/10.1186/s13018-015-0283-8.

Caiti, G., Dobbe, J.G.G., Bervoets, E., Beerens, M., Strackee, S.D., Strijkers, G.J., Streekstra, G.J., 2019. Biomechanical considerations in the design of patient-specific fixation plates for the distal radius. Med. Biol. Eng. Comput. 57, 1099–1107. https://doi.org/10.1007/s11517-018-1945-6.

Chevalier, Y., 2015. Numerical methodology to evaluate the effects of bone density and cement augmentation on fixation stiffness of bone-anchoring devices. J. Biomech. Eng. 137, 1–10. https://doi.org/10.1115/1.4030943.

Daszkiewicz, K., Maquer, G., Zysset, P.K., 2017. The effective elastic properties of human trabecular bone may be approximated using micro-finite element analyses of embedded volume elements. Biomech. Model. Mechanobiol. 16, 731–742. https://doi.org/10.1007/s10237-016-0849-3.

Einafshar, M., Hashemi, A., van Lenthe, G.H., 2021. Homogenized finite element models can accurately predict screw pull-out in continuum materials, but not in porous materials. Comput. Methods Progr. Biomed., 105966 https://doi.org/10.1016/j.cmpb.2021.105966.

Flaig, C., Arbenz, P., 2011. A scalable memory efficient multigrid solver for micro-finite element analyses based on CT images. Parallel Comput. 37, 846–854. https://doi.org/10.1016/j.parco.2011.08.001.

Gross, T., Pahr, D.H., Zysset, P.K., 2013. Morphology-elasticity relationships using decreasing fabric information of human trabecular bone from three major anatomical locations. Biomech. Model. Mechanobiol. 12, 793–800. https://doi.org/10.1007/s10237-012-0443-2.

Hambli, R., 2013. Micro-CT finite element model and experimental validation of trabecular bone damage and fracture. Bone 56, 363–374. https://doi.org/10.1016/j.bone.2013.06.028.

Helgason, B., Gilchrist, S., Ariza, O., Vogt, P., Enns-Bray, W., Widmer, R.P., Fitze, T., Pálsson, H., Pauchard, Y., Guy, P., Ferguson, S.J., Cripton, P.A., 2016. The influence of the modulus-density relationship and the material mapping method on the simulated mechanical response of the proximal femur in side-ways fall loading configuration. Med. Eng. Phys. 38, 679–689. https://doi.org/10.1016/j.medengphy.2016.03.006.

Hosseini, H.S., Dünki, A., Fabech, J., Stauber, M., Vilayphiou, N., Pahr, D., Pretterklieber, M., Wandel, J., Rietbergen, B. van, Zysset, P.K., 2017. Fast estimation of Colles' fracture load of the distal section of the radius by homogenized finite element analysis based on HR-pQCT. Bone 97, 65–75. https://doi.org/10.1016/j.bone.2017.01.003.

Inzana, J.A., Varga, P., Windolf, M., 2016. Implicit modeling of screw threads for efficient finite element analysis of complex bone-implant systems. J. Biomech. 49, 1836–1844. https://doi.org/10.1016/j.jbiomech.2016.04.021.

Kazmers, N.H., Judson, C.H., Presson, A.P., Xu, Y., Tyser, A.R., 2018. Evaluation of factors driving cost variation for distal radius fracture open reduction internal fixation. J. Hand Surg. Am. 43, 606–614.e1. https://doi.org/10.1016/j.jhsa.2018.04.015.

Kim, H., Lee, W., Choi, S.H., Kholinne, E., Lee, E., Alzahrani, W.M., Koh, K.H., Jeon, I.H., Kim, S., 2020. Role of additional inferomedial supporting screws in osteoporotic 3-Part Proximal humerus fracture: finite element analysis. Geriatr. Orthop. Surg. Rehabil. 11, 1–9. https://doi.org/10.1177/2151459320956958.

Knežević, J., Kodvanj, J., Čukelj, F., Pamuković, F., Pavić, A., 2017. A biomechanical comparison of four fixed-angle dorsal plates in a finite element model of dorsally-unstable radius fracture. Injury 48, S41–S46. https://doi.org/10.1016/S0020-1383(17)30738-6.

Kralinger, F., Blauth, M., Goldhahn, J., Kach, K., Voigt, C., Platz, A., Hanson, B., 2014. The influence of local bone density on the outcome of one hundred and fifty proximal humeral fractures treated with a locking plate. J. Bone Jt. Surg. 96, 1026–1032. https://doi.org/10.2106/JBJS.M.00028.

Lewis, G.S., Mischler, D., Wee, H., Reid, J.S., Varga, P., 2021. Finite element analysis of fracture fixation. Curr. Osteoporos. Rep. 19, 403–416. https://doi.org/10.1007/s11914-021-00690-y.

Li, J., Qin, L., Yang, K., Ma, Z., Wang, Y., Cheng, L., Zhao, D., 2020. Materials evolution of bone plates for internal fixation of bone fractures: a review. J. Mater. Sci. Technol. 36, 190–208. https://doi.org/10.1016/j.jmst.2019.07.024.

Li, Y., Zhou, Y., Zhang, X., Tian, D., Zhang, B., 2019. Incidence of complications and secondary procedure following distal radius fractures treated by volar locking plate (VLP). J. Orthop. Surg. Res. 14, 295. https://doi.org/10.1186/s13018-019-1344-1.

Lin, L.I.-K., 1989. A concordance correlation coefficient to evaluate reproducibility. Biometrics 45, 255. https://doi.org/10.2307/2532051.

Marangalou, J.H., Ito, K., van Rietbergen, B., 2012. A new approach to determine the accuracy of morphology-elasticity relationships in continuum FE analyses of human proximal femur. J. Biomech. 45, 2884–2892. https://doi.org/10.1016/j.jbiomech.2012.08.022.

Mischler, D., Windolf, M., Gueorguiev, B., Nijs, S., Varga, P., 2020. Computational optimization of screw orientations for improved locking plate fixation of proximal humerus fractures. J. Orthop. Transl. https://doi.org/10.1016/j.jot.2020.02.007.

Ovesy, M., Indermaur, M., Zysset, P.K., 2019. Prediction of insertion torque and stiffness of a dental implant in bovine trabecular bone using explicit micro-finite element analysis. J. Mech. Behav. Biomed. Mater. 98, 301–310. https://doi.org/10.1016/j.jmbbm.2019.06.024.

Ovesy, M., Voumard, B., Zysset, P., 2018. A nonlinear homogenized finite element analysis of the primary stability of the bone–implant interface. Biomech. Model. Mechanobiol. 17, 1471–1480. https://doi.org/10.1007/s10237-018-1038-3.

Pahr, D.H., Zysset, P.K., 2009. A comparison of enhanced continuum FE with micro FE models of human vertebral bodies. J. Biomech. 42, 455–462. https://doi.org/10.1016/j.jbiomech.2008.11.028.

Pahr, D.H., Zysset, P.K., 2008. Influence of boundary conditions on computed apparent elastic properties of cancellous bone. Biomech. Model. Mechanobiol. 7, 463–476. https://doi.org/10.1007/s10237-007-0109-7.

Panyasantisuk, J., Pahr, D.H., Gross, T., Zysset, P.K., 2015. Comparison of mixed and kinematic uniform boundary conditions in homogenized elasticity of femoral trabecular bone using microfinite element analyses. J. Biomech. Eng. 137, 011002 https://doi.org/10.1115/1.4028968.

Rice, J.C., Cowin, S.C., Bowman, J.A., 1988. On the dependence of the elasticity and strength of cancellous bone on apparent density. J. Biomech. 21, 155–168. https://doi.org/10.1016/0021-9290(88)90008-5.

Schader, J.F., Mischler, D., Dauwe, J., Richards, R.G., Gueorguiev, B., Varga, P., 2022. One size may not fit all: patient-specific computational optimization of locking plates for improved proximal humerus fracture fixation. J. Shoulder Elbow Surg. 31, 192–200. https://doi.org/10.1016/j.jse.2021.06.012.

Sensale, M., Vendeuvre, T., Schilling, C., Grupp, T., Rochette, M., Dall'Ara, E., 2021. Patient-specific finite element models of posterior pedicle screw fixation: effect of screw's size and geometry. Front. Bioeng. Biotechnol. 9, 175 https://doi.org/10.3389/FBIOE.2021.643154/XML/NLM.

Steiner, J.A., Christen, P., Affentranger, R., Ferguson, S.J., van Lenthe, G.H., 2017. A novel in silico method to quantify primary stability of screws in trabecular bone. J. Orthop. Res. 35, 2415–2424. https://doi.org/10.1002/jor.23551.

Steiner, J.A., Ferguson, S.J., van Lenthe, G.H., 2015. Computational analysis of primary implant stability in trabecular bone. J. Biomech. 48, 807–815. https://doi.org/10.1016/j.jbiomech.2014.12.008.

Steiner, J.A., Hofmann, U.A.T., Christen, P., Favre, J.M., Ferguson, S.J., van Lenthe, G.H., 2018. Patient-specific in silico models can quantify primary implant stability in elderly human bone. J. Orthop. Res. 36, 954–962. https://doi.org/10.1002/jor.23721.

Stipsitz, M., Zysset, P.K., Pahr, D.H., 2021. Prediction of the inelastic behaviour of radius segments: damage-based nonlinear micro finite element simulation vs pistoia criterion. J. Biomech. 116, 110205 https://doi.org/10.1016/j.jbiomech.2020.110205.

Stipsitz, M., Zysset, P.K., Pahr, D.H., 2020. Efficient Materially Nonlinear FE Solver for Simulations of Trabecular Bone Failure, vol. 19, pp. 861–874. https://doi.org/10.1007/s10237-019-01254-x.

Synek, A., Baumbach, S.F., Pahr, D.H., 2021. Towards optimization of volar plate fixations of distal radius fractures: using finite element analyses to reduce the number of screws. Clin. Biomech. 82 https://doi.org/10.1016/j.clinbiomech.2021.105272.

Synek, A., Chevalier, Y., Baumbach, S.F., Pahr, D.H., 2015. The influence of bone density and anisotropy in finite element models of distal radius fracture osteosynthesis: evaluations and comparison to experiments. J. Biomech. 48, 4116–4123. https://doi.org/10.1016/j.jbiomech.2015.10.012.

van Rietbergen, B., Ito, K., 2015. A survey of micro-finite element analysis for clinical assessment of bone strength: the first decade. J. Biomech. 48, 832–841. https://doi.org/10.1016/j.jbiomech.2014.12.024.

Varga, P., Grünwald, L., Inzana, J.A., Windolf, M., 2017. Fatigue failure of plated osteoporotic proximal humerus fractures is predicted by the strain around the proximal screws. J. Mech. Behav. Biomed. Mater. 75, 68–74. https://doi.org/10.1016/J.JMBBM.2017.07.004.

Virtanen, P., Gommers, R., Oliphant, T.E., Haberland, M., Reddy, T., Cournapeau, D., Burovski, E., Peterson, P., Weckesser, W., Bright, J., van der Walt, S.J., Brett, M., Wilson, J., Millman, K.J., Mayorov, N., Nelson, A.R.J., Jones, E., Kern, R., Larson, E., Carey, C.J., Polat, İ., Feng, Y., Moore, E.W., VanderPlas, J., Laxalde, D., Perktold, J., Cimrman, R., Henriksen, I., Quintero, E.A., Harris, C.R., Archibald, A.M., Ribeiro, A. H., Pedregosa, F., van Mulbregt, P., Vijaykumar, A., Bardelli, A., Pietro Rothberg, A., Hilboll, A., Kloeckner, A., Scopatz, A., Lee, A., Rokem, A., Woods, C.N., Fulton, C., Masson, C., Häggström, C., Fitzgerald, C., Nicholson, D.A., Hagen, D.R., Pasechnik, D.V., Olivetti, E., Martin, E., Wieser, E., Silva, F., Lenders, F., Wilhelm, F., Young, G., Price, G.A., Ingold, G.L., Allen, G.E., Lee, G.R., Audren, H., Probst, I., Dietrich, J.P., Silterra, J., Webber, J.T., Slavič, J., Nothman, J., Buchner, J., Kulick, J., Schönberger, J.L., de Miranda Cardoso, J.V., Reimer, J., Harrington, J., Rodríguez, J.L.C., Nunez-Iglesias, J., Kuczynski, J., Tritz, K., Thoma, M., Newville, M., Kümmerer, M., Bolingbroke, M., Tartre, M., Pak, M., Smith, N.J., Nowaczyk, N., Shebanov, N., Pavlyk, O., Brodtkorb, P.A., Lee, P., McGibbon, R.T., Feldbauer, R., Lewis, S., Tygier, S., Sievert, S., Vigna, S., Peterson, S., More, S., Pudlik, T., Oshima, T., Pingel, T.J., Robitaille, T.P., Spura, T., Jones, T.R., Cera, T., Leslie, T., Zito, T., Krauss, T., Upadhyay, U., Halchenko, Y.O., Vázquez-Baeza, Y., 2020. SciPy 1.0: fundamental algorithms for scientific computing in Python. Nat. Methods 173 17, 261–272. https://doi.org/10.1038/s41592-019-0686-2, 2020.

Wirth, A.J., Goldhahn, J., Flaig, C., Arbenz, P., Müller, R., van Lenthe, G.H., 2011. Implant stability is affected by local bone microstructural quality. Bone 49, 473–478.

Wirth, A.J., Müller, R., Harry van Lenthe, G., 2012. The discrete nature of trabecular bone microarchitecture affects implant stability. J. Biomech. 45, 1060–1067.

Yan, L., Lim, J.L., Lee, J.W., Tia, C.S.H., O'Neill, G.K., Chong, D.Y.R., 2020. Finite element analysis of bone and implant stresses for customized 3D-printed orthopaedic implants in fracture fixation. Med. Biol. Eng. Comput. 58, 921–931. https://doi.org/10.1007/s11517-019-02104-9.

Zysset, P.K., Curnier, A., 1995. An alternative model for anisotropic elasticity based on fabric tensors. Mech. Mater. 21, 243–250. https://doi.org/10.1016/0167-6636(95)00018-6.